

# Low Profile, High Gain and Wideband Circularly Polarized Antennas Using Hexagonal Shape Parasitic Patches

Shishir D. Jagtap<sup>1, \*</sup>, Rajashree Thakare<sup>2</sup>, and Rajiv K. Gupta<sup>3</sup>

**Abstract**—This paper proposes low profile, high gain and wideband circularly polarized (CP) microstrip antennas (MSA), using gap coupled parasitic patches (PPs) on superstrate layer. Printed and suspended probe fed, CP MSAs are designed on a 1.59 mm thick FR4 substrate, and an array of closely spaced hexagonal PPs are printed on the bottom side of the 1.59 mm thick FR4 superstrate and placed at a height about  $\lambda_0/8$  above the ground plane, where  $\lambda_0$  is the free space wavelength, corresponding to the central frequency of the operating frequency band. The gap coupled hexagonal PPs are not only used to enhance the axial ratio bandwidth (AR BW) and gain of the antenna, but also used to reduce impedance and gain variation of the antenna over the operating frequency band. ‘Ant9’ is a suspended MSA with 7 hexagonal PPs. A prototype ‘Ant9’ is fabricated and tested, which provides a peak gain of 9 dBi,  $S_{11} < -10$  dB, gain variation  $< 1$  dB, and AR  $< 3$  dB over 4.9 to 6.45 GHz frequency band. ARBW of 27.3% is achieved. The proposed ‘Ant9’ covers three frequency bands viz., 5.15 to 5.35 GHz, WLAN band, 5.725 to 5.875 GHz, ISM band, and 5.9 to 6.4 GHz, Satellite C band. The space fed antenna configuration reduces the cross polar radiation level (CPL) and increases the efficiency of the antenna. The measured results agree with the simulation ones. The overall size of ‘Ant9’ is  $0.96\lambda_0 \times 0.96\lambda_0 \times 0.136\lambda_0$ .

## 1. INTRODUCTION

Antennas are the fundamental component of any wireless system. CP antennas have many advantages over linearly polarized (LP) antennas. However, the design of a compact, directive and wideband CP antenna is always challenging, as compared to LP antenna. A single diagonal fed CP MSA is compact and simple to design; however, it provides narrow ARBW. A multi-fed CP antenna provides more AR BW than a single fed antenna. However, it increases the design complexity and cost of the antenna. Several BW enhancement techniques have been reported in [1–12, 14–16]. The AR BW of a CP MSA can be increased by using a thick and low permittivity dielectric substrate. A wideband single fed CP stacked MSA is proposed in [1]. It comprises a single diagonal fed MSA, with PP placed above the antenna. The antenna offers a peak gain of 7.5 dBi and ARBW of 13.5%. The AR BW of CP MSA is enhanced by using a multilayer aperture coupled antenna configuration in [2]. The aperture coupled PPs are printed on stacked dielectric layers, with each one being rotated by  $30^\circ$  from other. The antenna provides an ARBW of 33.6% and peak gain of 8 dBi; however, the antenna design is complex and has high profile with high SLL and low F/B lobe ratio.

A wideband single feed, truncated square patch CP antenna with PPs has been reported in [3]. Five square PPs are placed above the antenna, and one PP is placed beside the antenna. A stub is also used to provide better impedance matching over wide BW. A wideband dual feed, square ring CP

---

Received 6 June 2019, Accepted 1 August 2019, Scheduled 16 August 2019

\* Corresponding author: Shishir Digamber Jagtap (shishir.jagtapd@gmail.com).

<sup>1</sup> Department of Electronics and Telecommunication, SIES Graduate School of Technology, Navi-Mumbai, India. <sup>2</sup> Department of Electronics and Telecommunication, Bharati Vidyapeeth College of Engineering, Navi-Mumbai, India. <sup>3</sup> Department of Electronics and Telecommunication, Terna Engineering College, Navi-Mumbai, India.

antenna with PPs is designed in [4]. Four square PPs are placed above the antenna, and an L-shaped parasitic patch is placed beside the antenna. However, dual feed CP antenna not only increases the design complexity, but also increases the CPL, as compared to single feed CP antenna.

A wideband slotted square CP MSA with a slotted PP placed above the antenna is proposed in [5]. The slot on the microstrip patch is used not only to provide circular polarization but also to reduce the size of the antenna. Several gain and BW enhancement techniques of LP and CP MSAs are reported in [6]. Proximity fed LP MSA, with stacked gap coupled patches and square ring antenna array, provides significant enhancement in gain and BW of the antenna; however, it suffers from high profile [7]. A non-radiating edge gap coupled MSA, using small size PPs, is designed to achieve wide BW [8]. A compact high gain  $2 \times 2$  gap coupled array antenna is also designed. Low profile, printed wideband antennas are designed in [9–12]. A printed, high gain and wideband LP Yagi antenna, using tapered dipole as a driven element with tapered reflector, is reported in [9]. A wideband and wide beam CP printed microstrip antenna is proposed in [10]. This antenna offers a peak gain about 6 dBi, and impedance BW greater than 50% is achieved.

A compact CP double ring Yagi like antenna is designed in [11]. A square ring is used as the driven element, and a hybrid coupler is used to excite orthogonal modes. A single feed, high gain, wideband printed CP Yagi array antenna formed by horizontally and vertically polarized array elements is proposed in [12]. However, its radiation pattern has significant undesired radiations. Fabry Perot antennas (FPAs) are popular for gain and BW enhancement [13–15]; however, FPAs have high profile. A CP MSA using space fed array antenna in FPC is also proposed in [13]. The gain and gain variation of FPA increases, with increase in number of space fed PPs on the PRS layer [13]. The use of shaped ground plane decreases the gain variation of FPA over the operating frequency band [14]. However, design of this antenna is complex. A hexagonal ring based reactive impedance surface as a ground plane is used for antenna miniaturization and ARBW enhancement in [16].

In this paper, a simple, probe fed, circularly polarized suspended MSA, using an array of gap coupled hexagonal parasitic patches, is proposed to increase the AR BW and gain of the antenna with small antenna size and cross polar radiation levels. Also, the antenna offers wide beamwidth in both azimuth and elevation planes and small gain variation over the operating frequency band. The following sections present antenna geometry and design theory of the printed and suspended MSA with hexagonal PPs.

## 2. PRINTED MSA DESIGN WITH HEXAGONAL PPS

The proposed antenna is developed systematically. The step by step evolution of the proposed antenna is shown in Fig. 1. A diagonal fed rectangular patch antenna is designed on a 1.59 mm thick FR4 dielectric substrate, and gap coupled hexagonal parasitic patches are fabricated on the bottom side of a 1.59 mm thick FR4 dielectric superstrate and placed at about  $0.11\lambda_0$  above the ground plane. The antenna is fed through a coaxial probe of  $50\Omega$ . The antenna structures, with and without parasitic patches, are optimised using method of moment based IE3D simulator.

## 3. ANTENNA DESIGN THEORY

Initially, a CP probe fed, nearly square patch antenna is designed on a 1.59 mm thick FR4 substrate to operate over 5.725 to 5.875 GHz frequency band. This antenna is termed as ‘Ant1’. The optimized ‘Ant1’ has patch dimensions of 11.3 mm  $\times$  12.1 mm on a square ground plane of side 40 mm. Its diagonal feed position is  $(x, y) = (2.1 \text{ mm}, 2.1 \text{ mm})$ . This ‘Ant1’ provides a peak gain of 4.8 dBi,  $S_{11} < -10 \text{ dB}$  over 5.5 to 6 GHz frequency band and AR  $< 3 \text{ dB}$  over 5.76 to 5.872 GHz frequency band. The global BW of 112 MHz is achieved. The overall size of ‘Ant1’ is  $0.77\lambda_0 \times 0.77\lambda_0 \times 0.03\lambda_0$ , where  $\lambda_0$  is the free space wavelength (mm), corresponding to 5.75 GHz.

Now, the 1.59 mm thick FR4 dielectric superstrate is placed above the patch at a height about  $0.11\lambda_0$  from the ground plane. This antenna structure is termed as ‘Ant2’. The dielectric superstrate not only reduces the phase variation of waves over operating frequency band but also confines the waves towards broadside direction. The decrease in the phase variation results in increased BW. The tendency of the waves to bend towards the normal when passing from a low permittivity medium to

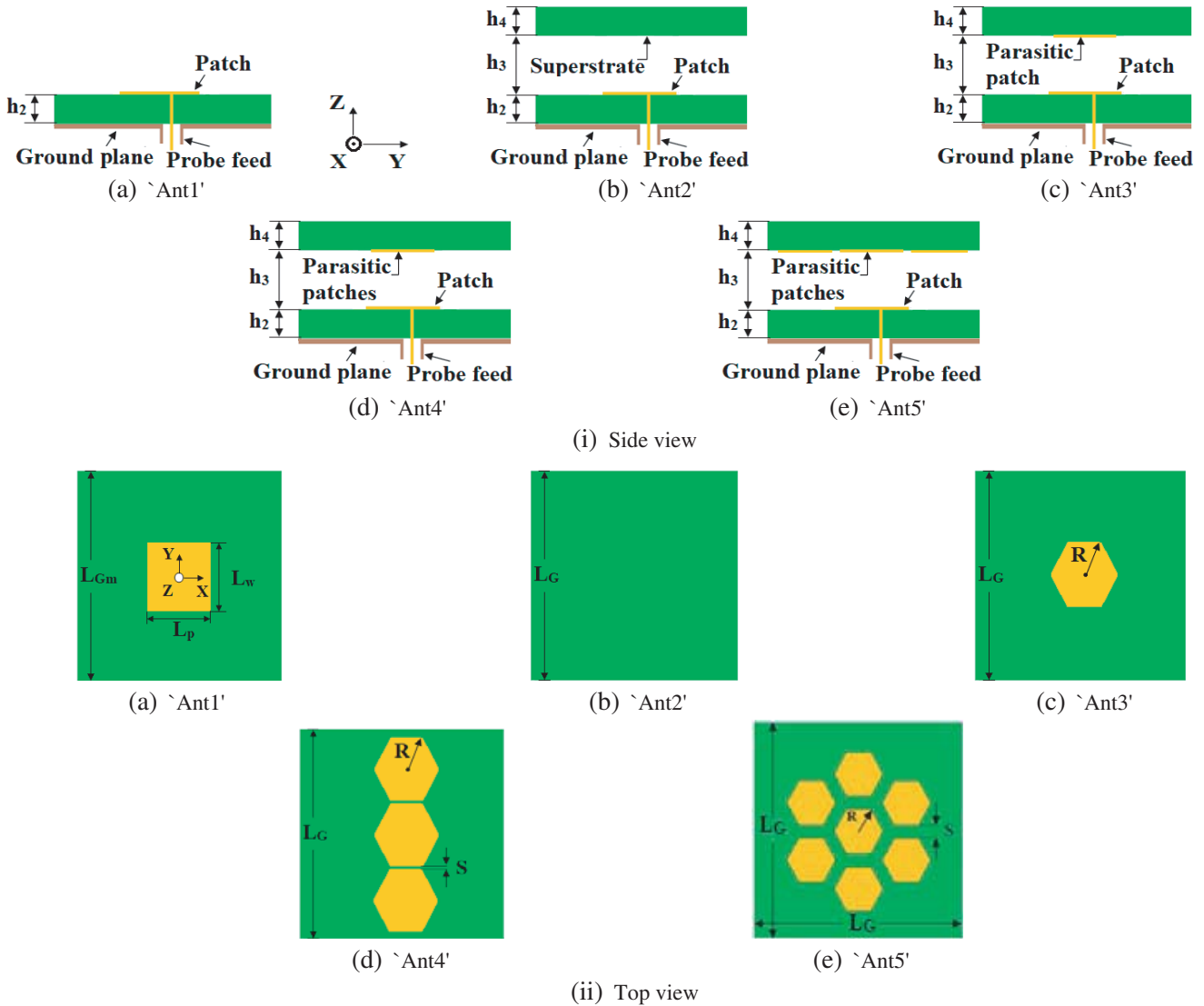


**Figure 1.** (i) Side view and (ii) top view of ‘Ant1’ to ‘Ant5’ ( $h_2 = h_4 = 1.59$ ,  $h_3 = 4.41$ ,  $L_p = 11.3$ ,  $L_w = 12.1$ ,  $R = 5.25$ ,  $S = 1$ ,  $L_{Gm} = 40$ ,  $L_G = 50$  (all dimensions are in mm)).

a high permittivity medium confines the wave towards broadside direction, which results in the gain enhancement of the antenna. ‘Ant2’ provides a peak gain of 6 dBi,  $S_{11} < -15$  dB over 5.5 to 6 GHz frequency band and  $AR < 3$  dB over 5.715 to 5.865 GHz frequency band. The global BW of 150 MHz is achieved. The overall size of ‘Ant2’ is  $0.96\lambda_0 \times 0.96\lambda_0 \times 0.145\lambda_0$ .

Thereafter, a single hexagonal parasitic patch (PP) inscribed in a circle of radius  $R$  is fabricated on the bottom side of an FR4 superstrate. This antenna structure is termed as ‘Ant3’. The optimised value of  $R$  is about  $0.25\lambda$ , where  $\lambda$  is the wavelength in dielectric. The space fed parasitic patch is equivalent to parallel L-C circuit. As the dielectric loaded shorted wave transmission between microstrip patch and the parasitic patch gives shunt inductance and shunt capacitance is formed between the parasitic patch and ground plane separated by dielectrics. Therefore, parasitic patch and ground plane together form a resonant cavity. The cavity resonant frequency is lower than the antenna resonant frequency. The cavity resonant frequency primarily depends on the size of the parasitic patch and the distance between parasitic patch and ground plane. The cavity inductance increases with increase in distance between the ground plane and parasitic patch, which in turn reduces the cavity resonant frequency and vice versa. The higher BW in ‘Ant3’ is achieved due to electromagnetic coupling between the antenna

resonant frequency and parasitic patch resonant frequency as shown in Fig. 2(a). ‘Ant3’ provides peak gain of 6.7 dBi,  $S_{11} < -15$  dB over 5.5 to 6 GHz frequency band, and AR < 3 dB over 5.63 to 5.84 GHz frequency band. The global BW of 210 MHz is achieved.

Now, to further increase the gain and BW of the antenna, two more hexagonal shape PPs are placed in close proximity, and this antenna is termed as ‘Ant4’. These patches form a gap coupled space fed array antenna. The gap coupled patches not only increase the BW and gain of the antenna but also reduces the size and gain variations of the antenna. The BW of this antenna depends on the gap between the PPs and its height from the antenna. The gap between the patches should be much smaller than the wavelength, when the driven element is narrow band antenna [6]. The inductance and capacitance of the cavity formed between PPs and ground plane increase, with increase in number of PPs. Also, capacitance is formed between parasitic patches. Therefore, with increase in parasitic patches on the superstrate, the overall L and C of the antenna increase, and consequently, the resonant frequency of the antenna decreases. The values of L and C can be controlled by adjusting the shape and size of the parasitic patch, gap between the parasitic patches, and distances of parasitic patches from antenna and ground plane. The cavity resonant frequency primarily depends on the size and shape of the PP, gap between PPs, and the distance between parasitic patch and ground plane. The antenna and parasitic patches couple electromagnetically and provide wide BW. The parametric study is carried out, to optimize and understand the impedance behaviour of the antenna structures. The effect of change in (a) spacing between ground plane and parasitic patch, (b) parasitic patch shape and size, and (c) the gap between the parasitic patches on the cavity resonance is studied. This antenna with 3 parasitic patches offers, a peak gain of 7.7 dBi,  $S_{11} < -10$  dB over 5.5 to 6 GHz frequency band and AR < 3 dB over 5.62 to 6.02 GHz frequency band. The global BW of 400 MHz is achieved.

‘Ant4’ is further modified by adding four more parasitic patches as shown in Fig. 1(e), which not only increases gain and BW of the antenna but also makes it more symmetric to have a broadside radiation. This antenna is termed as ‘Ant5’. This antenna with 7 patches offers, a peak gain of 8.8 dBi,  $S_{11} < -20$  dB over 5.5 to 6 GHz frequency band, and AR < 3 dB over 5.46 to 6.01 GHz frequency band. The global BW of 550 MHz is achieved. The gain variation < 0.5 dB over the operating frequency band is achieved. ‘Ant5’ also provides gain enhancement of 2.8 dBi and BW enhancement of 400 MHz over ‘Ant2’.

$S_{11}$  and antenna efficiency of ‘Ant1’ to ‘Ant5’ structures are shown in Fig. 2. The gain and AR BW of these antennas increase, with increase in number of PPs on superstrate layer, as shown in Fig. 3. The gain of the antenna increases from 4.8 dBi to 8.8 dBi for ‘Ant1’ to ‘Ant5’. ARBW of these antennas increases from 112 MHz to 550 MHz for ‘Ant1’ to ‘Ant5’. The gain variation of ‘Ant5’ over 5.5 to 6 GHz frequency band is only about 0.4 dB. The real and imaginary parts of impedance variations of these antennas are shown in Fig. 4, and the impedance variation of the antenna decreases with increase in number of hexagonal patches on the superstrate layer. ‘Ant5’ has maximum number of parasitic patches; therefore, it has very little variation in the impedance as shown in Fig. 4. Flat  $S_{11} < -20$  dB

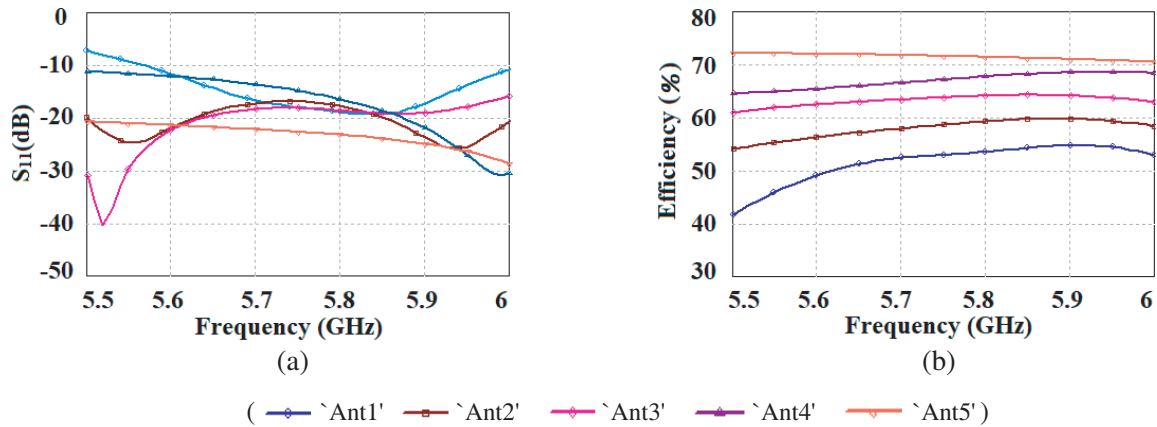


**Figure 2.** (a)  $S_{11}$  (dB) and (b) efficiency variation vs. frequency.

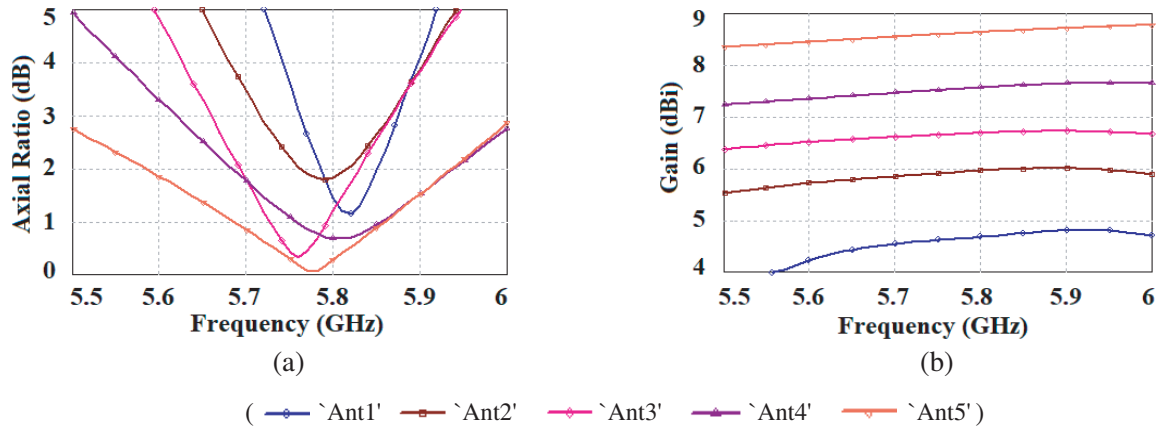


Figure 3. (a) Gain and (b) AR variation vs. frequency.

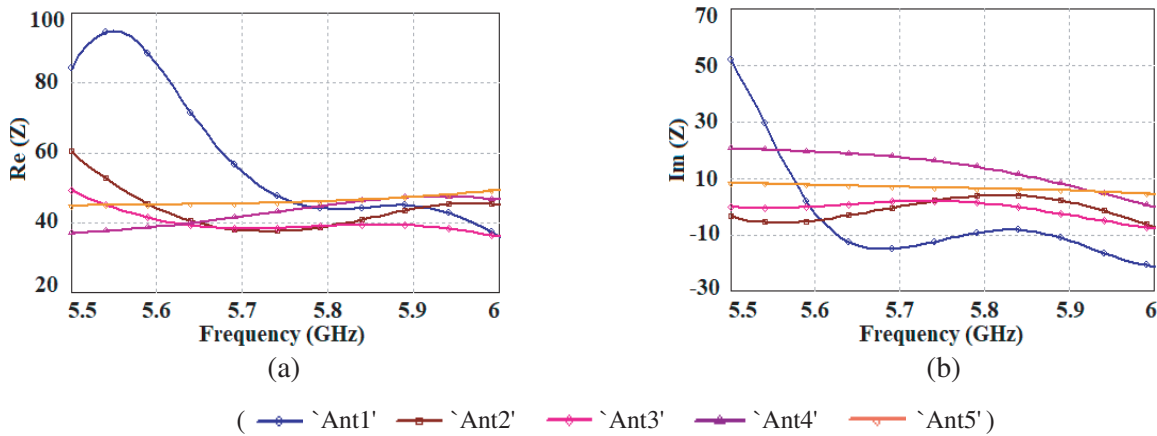


Figure 4. Impedance variations (a) real and (b) imaginary part of impedance.

is achieved in ‘Ant5’, which in turn reduces gain variation of ‘Ant5’.

The radiation patterns of ‘Ant1’ to ‘Ant5’ are shown in Fig. 5. The proposed antenna is a gap coupled space fed array antenna; therefore, it does not include a feed line network to feed the antenna elements, which reduces cross polar radiations due to feed line network. The radiation characteristics of ‘Ant1’ to ‘Ant5’ are tabulated in Table 1.  $CPL < -16$  dB is achieved in all the antenna structures

#### 4. DESIGN THEORY OF PARASITIC PATCHES

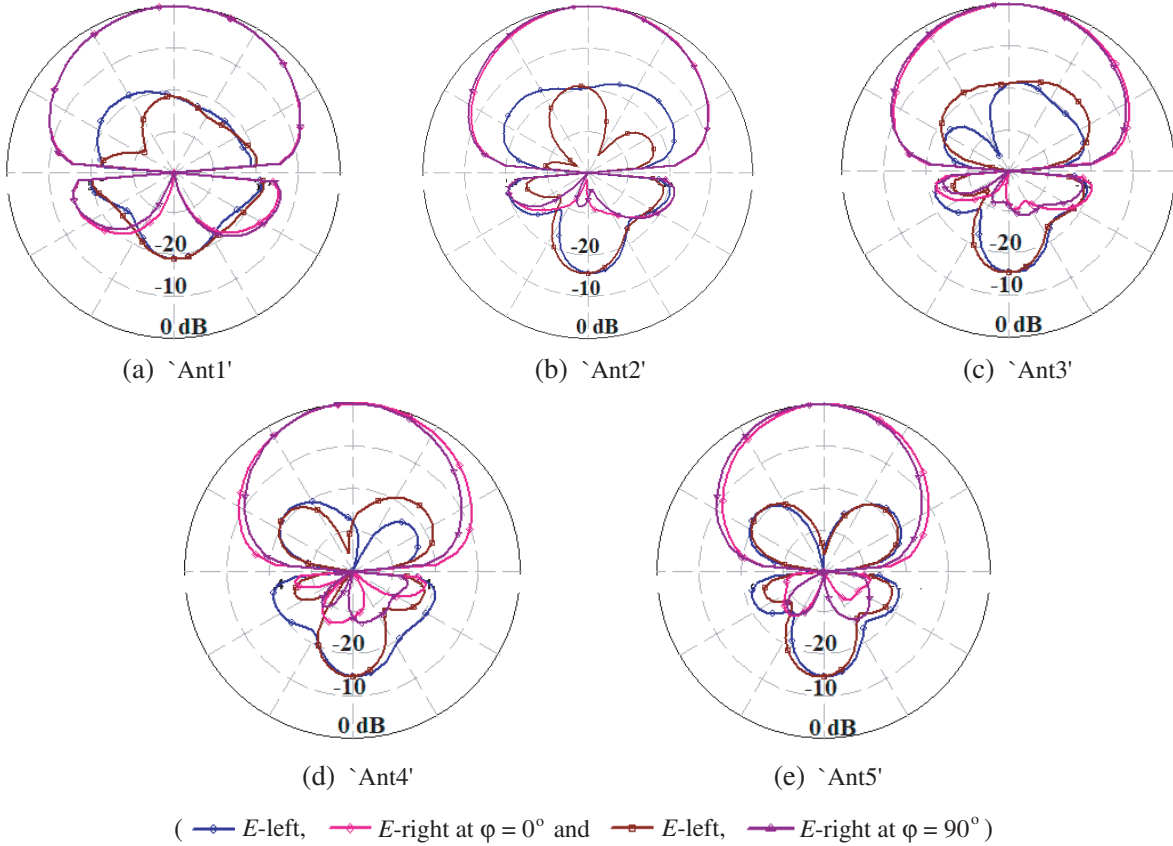
MSA with hexagonal PPs provides better ARBW than square PPs. Since the hexagonal PP provides rotation to the current induced in the patch, thereby, giving circular polarization over wide band. These PPs are space fed antenna elements; therefore, initially, a hexagonal patch inscribed in circle of radius  $R = 0.25\lambda$  is designed, where  $\lambda$  is the wavelength in dielectric at frequency 5.8 GHz. The side of the patch is optimized to achieve wide BW response.

Also, antenna with circular PPs is symmetric; however, the gap between patches will not be uniform, which may cause tilt in radiation pattern from broadside direction. Therefore, hexagonal shaped PPs are preferred over other shapes. The current distributions of the proposed antenna with square and hexagonal PPs are shown in Fig. 6 and Fig. 7, respectively.

ARBW is further enhanced by designing a simple, probe fed, CP suspended MSA, using space fed array of gap coupled hexagonal PPs. The proposed antenna offers ultra-wide BW and wide beamwidths in both azimuth and elevation planes with less gain variation over the operating frequency band. The

**Table 1.** Radiation parameter of Ant1 to Ant5 structures at 5.8 GHz.

Antenna	Gain (dBi)	$S_{11} < -10$ dB BW (MHz)	AR BW (MHz)	CPL (dB)	Antenna size (mm <sup>3</sup> )
'Ant1'	4.8	> 435 MHz (5.56 to 6 GHz)	112 MHz	-18.2	40 × 40 × 1.59
'Ant2'	6	> 500 MHz (5.5 to 6 GHz)	150 MHz	-16	50 × 50 × 7.59
'Ant3'	6.7	> 500 MHz (5 to 6 GHz)	210 MHz	-17.2	50 × 50 × 7.59
'Ant4'	7.7	> 500 MHz (5 to 6 GHz)	400 MHz	-17.8	50 × 50 × 7.59
'Ant5'	8.8	> 500 MHz (5 to 6 GHz)	550 MHz	-18.5	50 × 50 × 7.59

**Figure 5.** Radiation patterns of antenna structures at 5.8 GHz.

following sections presents the antenna geometry, design theory, antenna analysis, and simulation, fabrication, and measurement results.

## 5. SUSPENDED MSA DESIGN WITH HEXAGONAL PPS

The step by step evolution of the proposed antenna is shown in Fig. 8. It comprises a diagonal fed rectangular patch antenna printed on a 1.59 mm thick FR4 dielectric substrate. The substrate is

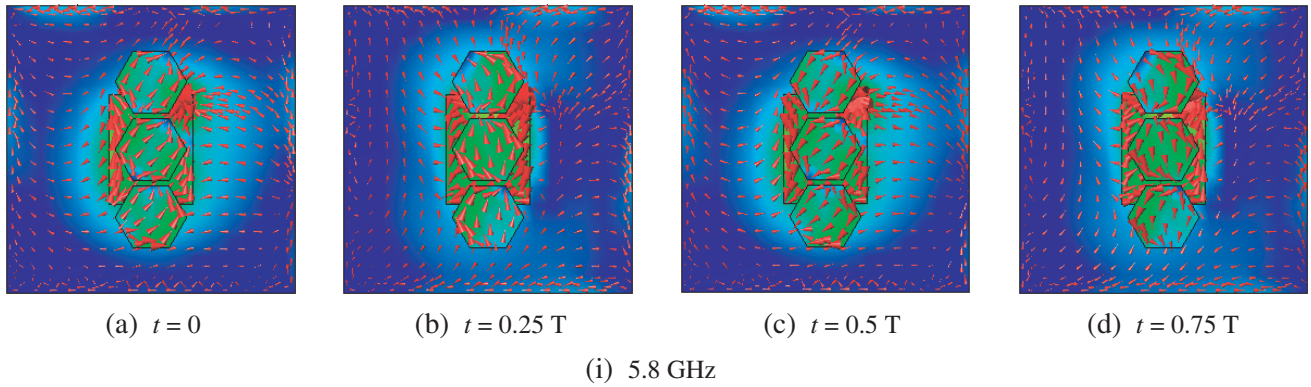


Figure 6. Current distribution of ‘Ant4’ with hexagonal patches.

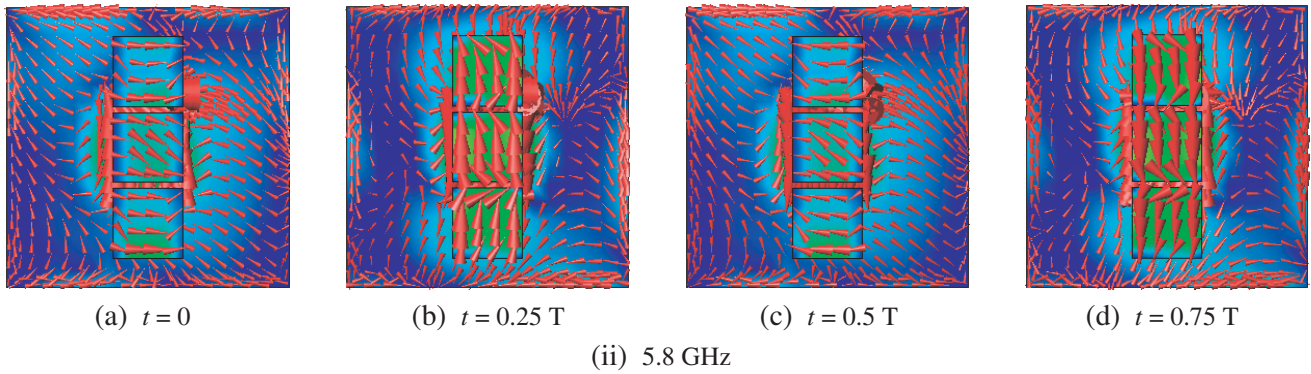


Figure 7. Current distribution of ‘Ant4’ with square patches.

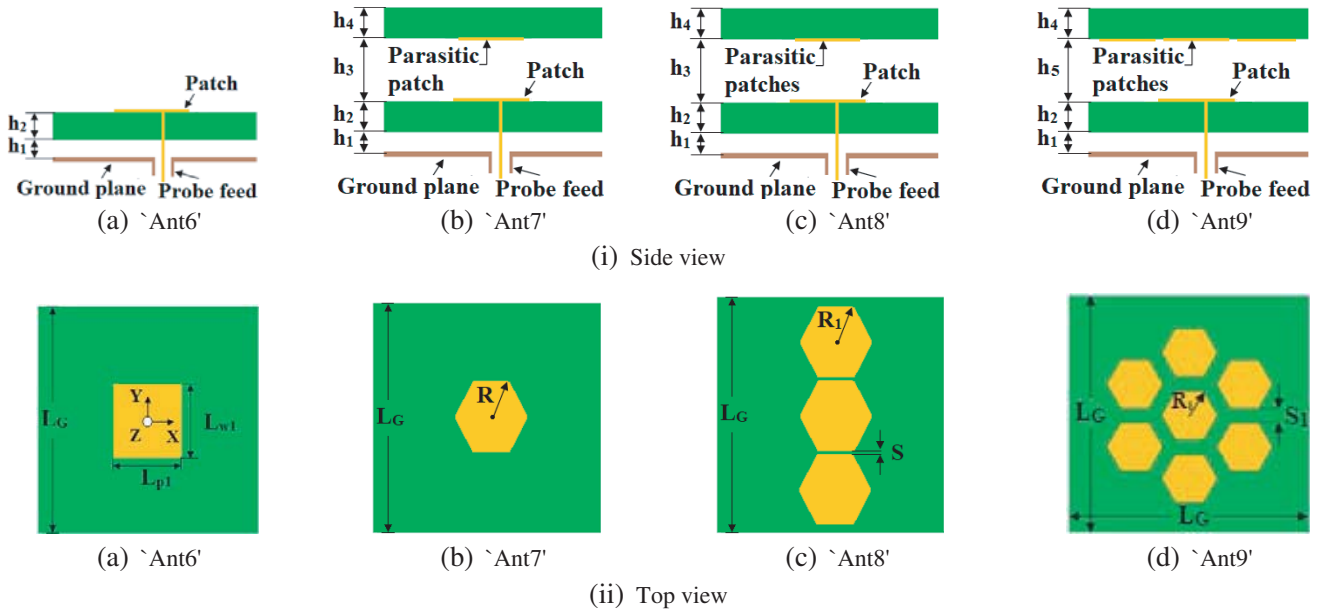
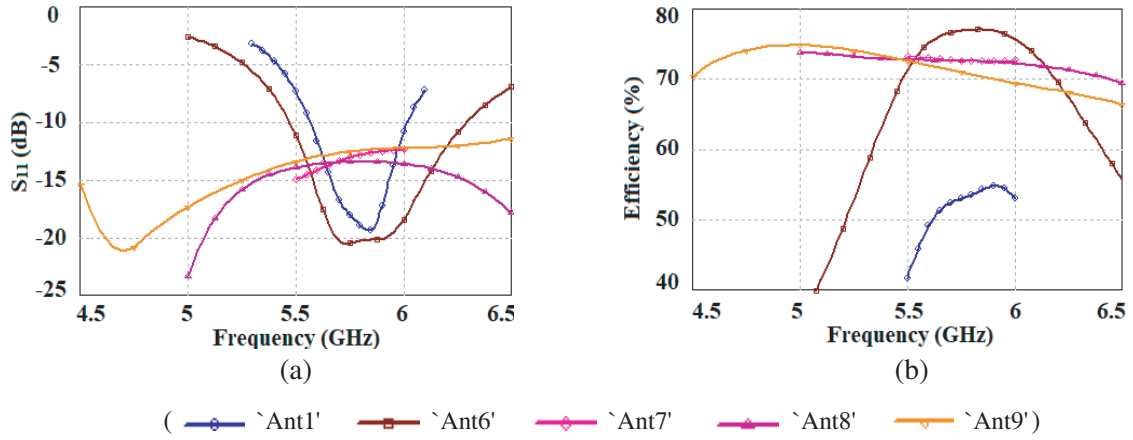


Figure 8. (i) Side view and (ii) top view of ‘Ant6’ to ‘Ant9’ ( $h_1 = 1$ ,  $h_2 = h_4 = 0.59$ ,  $L_{p1} = 14$ ,  $L_{w1} = 16$ ,  $h_3 = 4.41$ ,  $h_5 = 3$ ,  $R = 6$ ,  $R_1 = 5.75$ ,  $S = 1$ ,  $S_1 = 3$ ,  $G = 50$  (all dimensions are in mm)).

suspended 1 mm above the ground plane, and the gap coupled hexagonal PPs are fabricated on the bottom side of a 1.59 mm thick FR4 dielectric superstrate and placed at about  $0.11\lambda_0$  above the ground plane. The antenna structure is fed through a coaxial probe of  $50\ \Omega$ . Initially, ‘Ant1’ discussed in Section 3 is modified to suspended MSA to improve the gain and ARBW of the antenna. A single probe fed CP MSA is designed on a 1.59 mm thick FR4 substrate and suspended at a height of 1 mm above the metal plated ground plane. This antenna is termed as ‘Ant6’. This ‘Ant6’ provides a peak gain of 7.67 dBi,  $S_{11} < -10$  dB over 5.47 to 6.29 GHz frequency band, and AR  $< 3$  dB over 5.64 to 5.82 GHz frequency band. The global BW of 180 MHz is achieved. The overall size of ‘Ant6’ is  $0.77\lambda_0 \times 0.77\lambda_0 \times 0.05\lambda_0$ .

Now, to increase ARBW, similar to the antenna design in Section 3, ‘Ant6’ is modified by placing a 1.59 mm thick FR4 dielectric superstrate at a height about  $0.13\lambda_0$  above the ground plane. An array of  $1 \times 1$ ,  $1 \times 3$ , and  $1 \times 7$  hexagonal shape PPs are printed on the bottom side of this FR4 superstrate, and these antennas are termed as Ant7’, ‘Ant8’, and ‘Ant9’, respectively. Hexagonal PPs are inscribed in circles of radii  $R$  and  $R_1$ . The optimised values of  $R$  and  $R_1$  are 6 mm and 5.75 mm, respectively. The overall size of ‘Ant7’ and ‘Ant8’ is  $50 \times 50 \times 8.59\ \text{mm}^3$ . The optimized dimensions of the ‘Ant9’ are — radius of the hexagonal PP is  $R_1 = 5.75$  mm; spacing between PPs is  $S_1 = 3$  mm; and height of the superstrate layer is  $h_3 = 3$  mm. The overall size of the ‘Ant9’ is reduced to  $50 \times 50 \times 7.18\ \text{mm}^3$ .

$S_{11}$  and efficiency variations of these antennas are shown in Fig. 9(a) and Fig. 9(b), respectively. Real and imaginary parts of impedance variations of ‘Ant1’ and ‘Ant6’ to ‘Ant9’ structures are shown in Fig. 10. Impedance variation of the antenna decreases, with increase in number of parasitic patches



**Figure 9.** (a)  $S_{11}$  (dB) and (b) antenna efficiency vs. frequency.

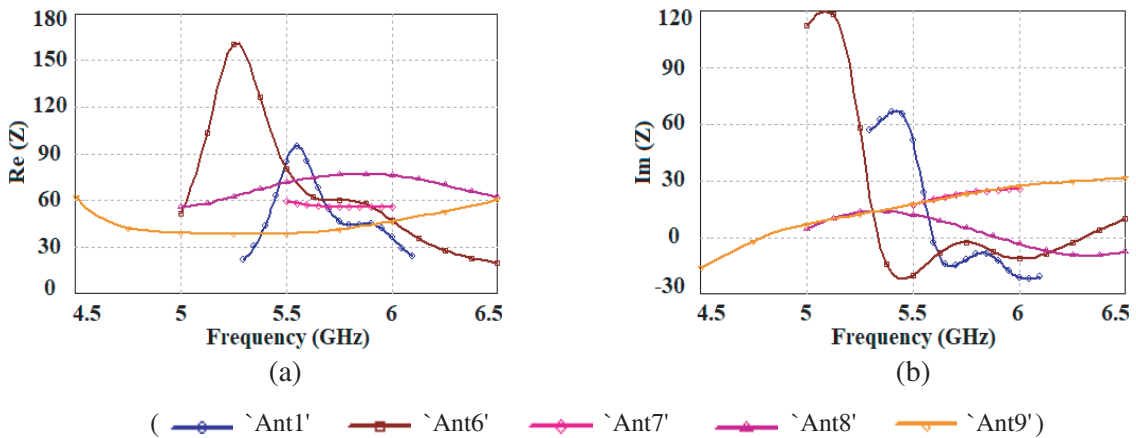


**Figure 10.** Impedance variations (a) real and (b) imaginary part of impedance.

on superstrate layer, as evident from Fig. 10.

The gain and AR variations of these antennas are shown in Fig. 11(a) and Fig. 11(b), respectively. The gain variation of ‘Ant8’ is  $< 0.5$  dB, and ‘Ant9’ is  $< 1$  dB, over the entire operating frequency band. ‘Ant9’ is designed with more parasitic patches than ‘Ant7’ and ‘Ant8’; therefore, it resonates at lower frequency as evident from Figs. 9(a) and 11(b), respectively. AR BW of the antenna increases significantly, with increase in parasitic patches on dielectric superstrate layer, as shown in Fig. 11(b).

The radiation patterns of ‘Ant8’ and ‘Ant9’ at 5.35 GHz, 5.8 GHz, and 6.15 GHz are shown in Fig. 12 and Fig. 13, respectively.  $CPL < -10.8$  dB is achieved over the wide frequency band. The gain of the antenna increases from 7.67 to 8.74 dBi, and half power beam width (HPBW) decrease from  $72.4^\circ$  to  $55^\circ$  with increase in PPs from  $1 \times 1$  to  $1 \times 7$ .  $E$  and  $H$  plane beamwidths are nearly same for ‘Ant6’ and ‘Ant7’, respectively as shown in Table 2. The radiation patterns of ‘Ant8’ and ‘Ant9’ tilt slightly from the broadside direction, due to its asymmetric antenna configuration. The distance from the microstrip patch to the PPs is not uniform; this introduces phase delay in the induced signal, which causes tilt in main lobe of a pattern from broadside direction.

In ‘Ant9’, the superstrate height is decreased; therefore, the path difference between the radiating edges of the microstrip patch and outer parasitic patches is significant, which therefore, introduces significant phase delay and causes tilt in the main beam of the radiation pattern as evident in Fig. 13. Also, at higher frequencies, wavelength is smaller. Therefore, the phase delay is significant at higher frequencies, and the radiation beam maxima tilt significantly from broadside direction at higher frequency, as evident in Fig. 12 and Fig. 13.

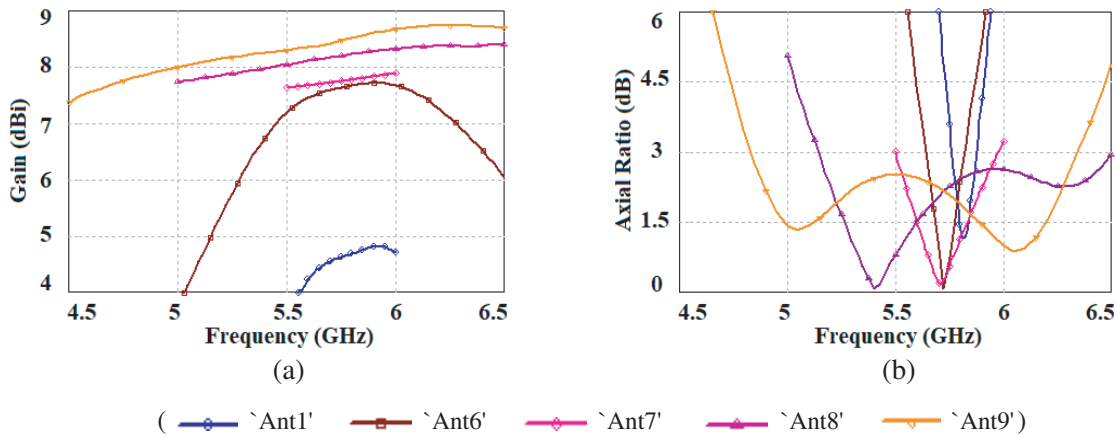


Figure 11. (a) Gain and (b) AR variation vs. frequency.

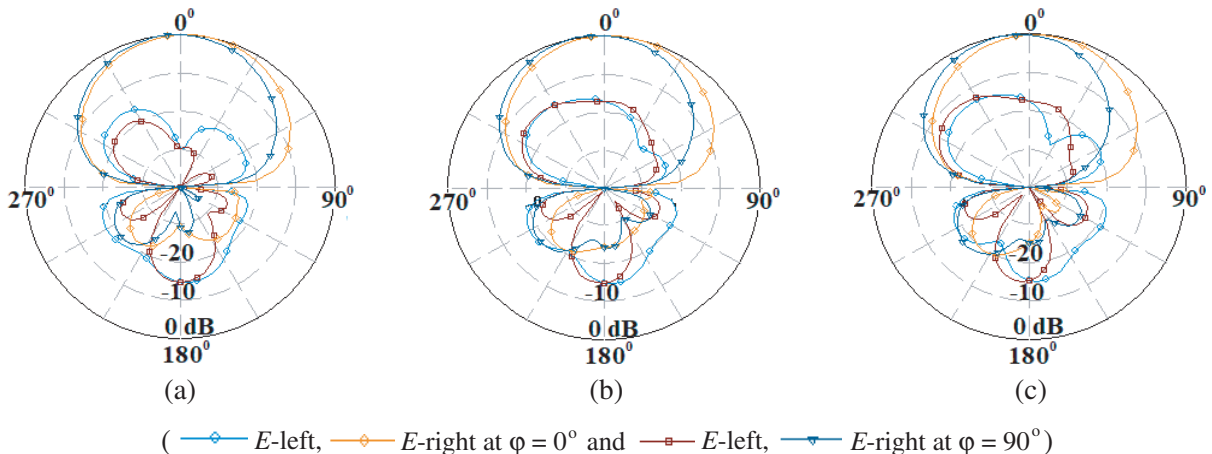
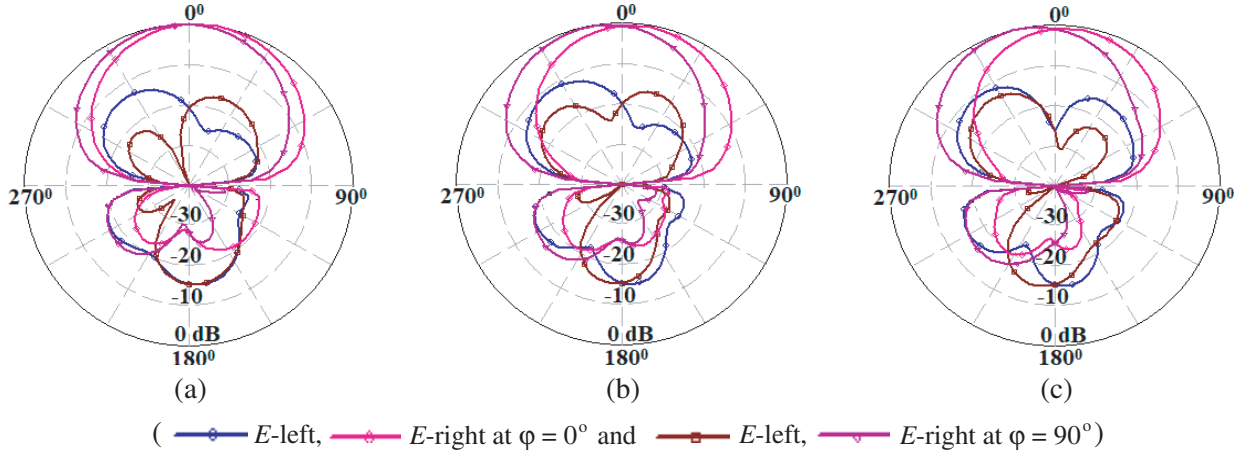


Figure 12. Radiation patterns of Ant8 at (a) 5.35 GHz, (b) 5.8 GHz and (c) 6.15 GHz.



**Figure 13.** Radiation patterns of ‘Ant9’ at (a) 5.35 GHz, (b) 5.8 GHz and (c) 6.15 GHz.

**Table 2.** Radiation parameters of the proposed antenna structure.

Ant	Gain (dBi)	$S_{11} < -10$ dB BW (MHz)	AR < 3 dB BW (MHz)	CPL (dB)	F/B (dB)	HPBW ( $E/H$ plane)	Antenna size (mm <sup>3</sup> )
‘Ant1’	4.74	> 435 MHz (5.56 to 6 GHz)	110 MHz (5.76 to 5.87 GHz)	-18.1	37	85.2°/85.2°	40 × 40 × 1.59
‘Ant6’	7.67	820 MHz (5.47 to 6.29 GHz)	180 MHz (5.66 to 5.84 GHz)	-18.3	35	72.4°/70.2°	50 × 50 × 2.59
‘Ant7’	7.87	1330 MHz (5.17 to 6.5 GHz)	470 MHz (5.5 to 5.97 GHz)	-15.2	28.8	66.4°/67°	50 × 50 × 8.59
‘Ant8’	8.4	> 1500 MHz (5 to 6.5 GHz)	1360 MHz (5.14 to 6.5 GHz)	-12.3	25.2	64.2°/58.7°	50 × 50 × 8.59
‘Ant9’	8.74	> 2000 MHz (4.5 to 6.5 GHz)	1510 MHz (4.84 to 6.35 GHz)	-10.9	25.8	55°/55.5°	50 × 50 × 7.18

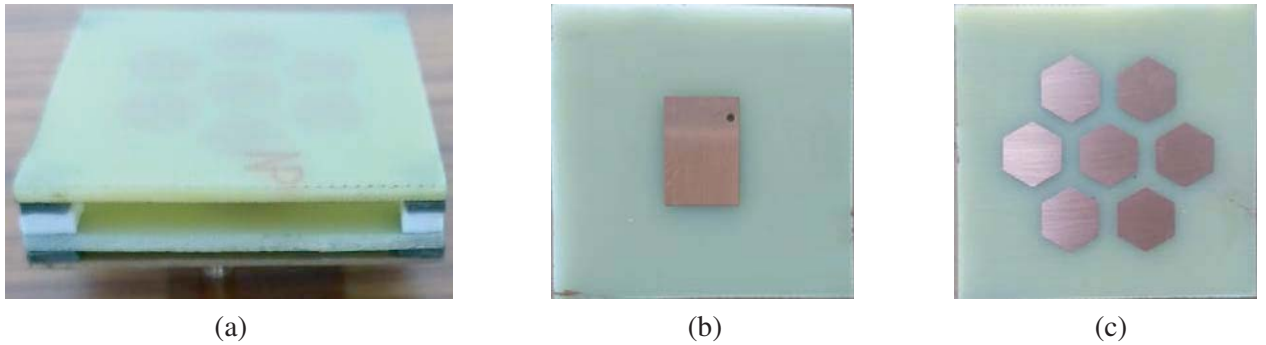


**Figure 14.** Photographs of the prototype ‘Ant8’ and ‘Ant9’. (a) Side view, (b) top view of MSA, (c) 7 hexagonal PPs.

## 6. FABRICATION AND MEASUREMENT RESULTS

A prototype structure of ‘Ant9’ is fabricated and tested. Photographs of the fabricated antenna are shown in Fig. 14. The simulated and measured  $S_{11}$ , AR, and gain variations of ‘Ant9’ are shown in

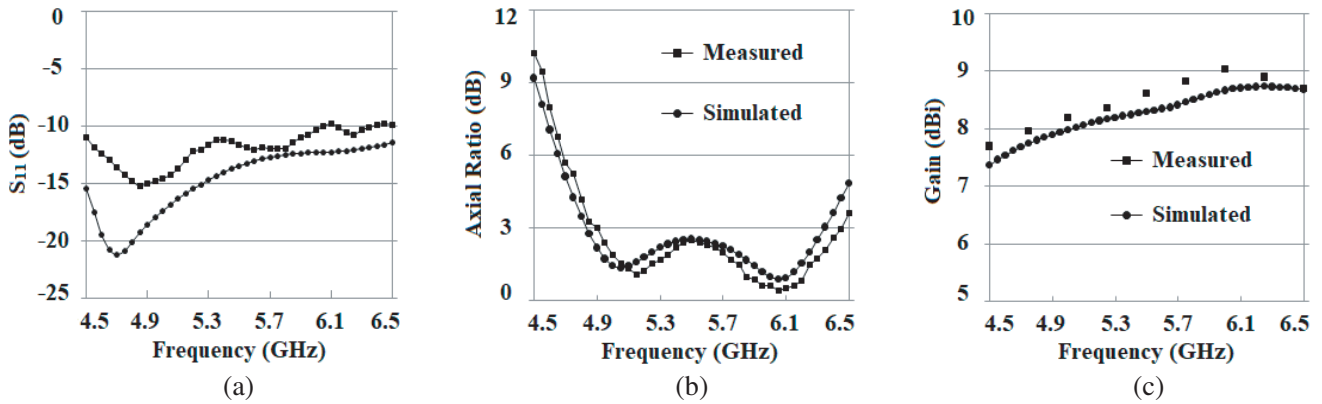


Figure 15. Simulated and measured (a)  $S_{11}$  (dB), (b) A.R and (c) gain vs. frequency of ‘Ant9’.

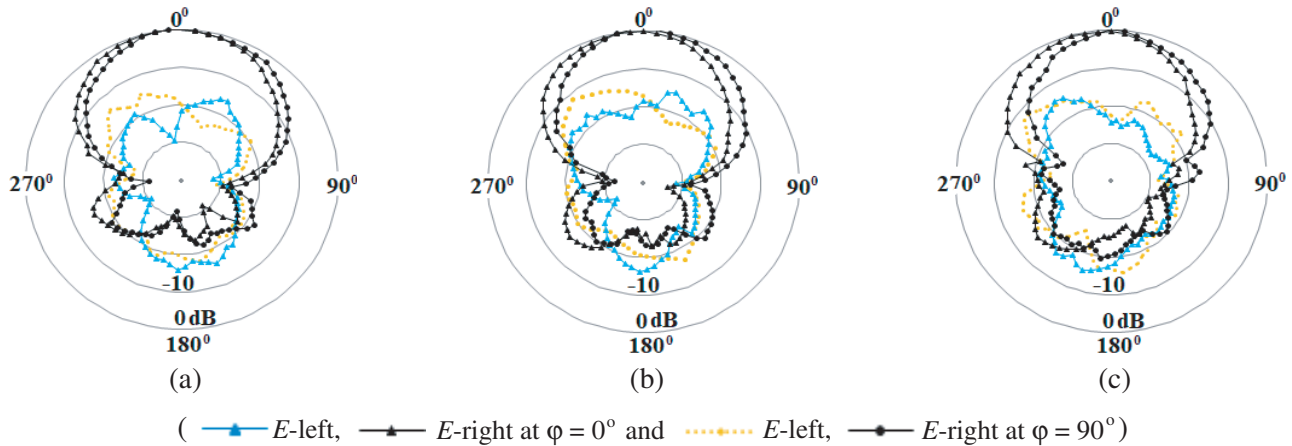


Figure 16. Measured radiation patterns of ‘Ant9’. (a) 5.25 GHz, (b) 5.8 GHz, (c) 6.15 GHz.

Fig. 15.

$S_{11} < -10$  dB, gain variation  $< 1$  dB, and AR  $< 3$  dB over 4.9 to 6.45 GHz frequency band are achieved. The measured radiation patterns of ‘Ant9’ at 5.25, 5.8, and 6.15 GHz are shown in Fig. 16. Broadside radiation patterns are obtained with little variation over the operating frequency band. The radiation patterns of ‘Ant9’ have SLL  $< -15$  dB, CPL  $< -10$  dB, and F/B lobe ratio  $> 25$  dB. CPLs of ‘Ant9’ are more than ‘Ant5’ due to longer probe feed length than ‘Ant5’. The variation in simulated and measured results may be attributed to fabrication errors and/or alignment errors. The variation may be accounted for dielectric constant variation of the available substrate and dielectric constant assigned to substrate and superstrate during simulation. Also the variation may be due to some errors in superstrate height.

The proposed ‘Ant9’ is compared with reported antennas as shown in Table 3. ‘Ant9’ has less gain variation over the operating band than the antennas in [1–5, 10–12]. The proposed antenna profile is smaller than the antenna in [1]. Also, the AR BW and gain of the proposed antenna are significantly larger than the antenna in [1]. The AR BW of the antenna in [2] is higher than the proposed antenna; however, the proposed antenna has low profile and offers higher gain with low SLL. The sizes of the antennas in [3, 5] are smaller than the proposed antenna. However, gain, AR BW, and SLL of the proposed antenna are superior to the antennas in [3, 5]. The antenna in [4] is compact and provides higher ARBW than the proposed antenna. However, the SLL, gain, and F/B lobe ratio of the proposed antenna are superior to the antenna in [4]. The antennas in [10–12] are in low profile; however, the proposed antenna provides significantly large gain and AR BW with low SLL, as compared to antenna in [10–12]. Also, the proposed antenna provides higher gain and lower SLL than the antennas in [10–12].

**Table 3.** Comparison of proposed antenna with reported antennas (NR — Not reported).

Reference Antenna	Radiation parameters of the antenna					
	Gain (dBi)	$S_{11} < -10$ dB BW (%)	AR BW (%)	SLL (dB)/CPL (dB)	F/B (dB)	Size of the antenna ( $\lambda_0^3$ )/Antenna profile ( $\lambda_0$ )
[1]	9	21	13.5	NR	NR	NR/ $0.15\lambda_0$
[2]	8 (dBic)	48	33.6	-2/NR	> 2	NR/ $0.34\lambda_0$
[3]	7.9	> 30	20.7	$\sim -9$ /NR	> 20	$0.81\lambda_0 \times 0.81\lambda_0 \times 0.09\lambda_0$
[4]	8.4	38	28.1	-9/-12	> 17	$0.82\lambda_0 \times 0.82\lambda_0 \times 0.08\lambda_0$
[5]	7 (dBic)	21	13.4	NR	> 14	$0.6\lambda_0 \times 0.6\lambda_0 \times 0.895\lambda_0$
[10]	$\sim 5$	> 9.5	11.3	$\sim (-10/-7)$	> 17	$1.55\lambda_0 \times 1.45\lambda_0 \times 0.03\lambda_0$
[11]	4.75	10.9	2.84	$\sim (-9$ /NR)	> 12	$0.25\lambda_0 \times 0.25\lambda_0 \times 0.0625\lambda_0$
[12]	8 (dBic)	13.1	10.51	$\sim (-9$ /NR)	> 12	$0.96\lambda_0 \times 1.13\lambda_0 \times 0.05\lambda_0$
[13]	17.3	> 8	2.6	-25/-26	> 20	$5\lambda_0 \times 5\lambda_0 \times 0.5\lambda_0$
‘Ant9’	9	> 35	27.3	-15.6/-10.8	> 20	$0.96\lambda_0 \times 0.96\lambda_0 \times 0.136\lambda_0$

The gain of the antenna in [13] is significantly large than the proposed antenna. However, this antenna has very large size and narrow AR BW.

## 7. CONCLUSION

A simple, compact, high gain, CP UWB MSA, using  $1 \times 7$  hexagonal shape PPs, is designed to operate over 5.15–5.35 GHz WLAN band, 5.725–5.875 GHz ISM band, and 5.9–6.4 GHz Satellite C band. ‘Ant9’ is a space fed array antenna, which avoids the design of a complex feed line network, losses, and cross polarization due to feed network. The superstrate layer used in the antenna structure acts as a radome to the antenna. ‘Ant9’ provides a peak gain of 9 dBi and 27.3% of AR BW. ‘Ant9’ also offers wide beamwidths in  $E$  and  $H$  planes.

## REFERENCES

1. Nasimuddin, K. P. Esselle, and A. K. Verma, “Wideband circularly polarized stacked microstrip antennas,” *IEEE Antennas and Wireless Propagation Letters*, Vol. 6, 21–24, 2007.
2. Oraizi, H. and R. Pazoki, “Wideband circularly polarized aperture-fed rotated stacked fed antenna,” *IEEE Transactions on Antennas and Propagation*, Vol. 61, No. 3, 1048–1054, 2013.
3. Yang, W., J.-Y. Zhou, Z. Yu, and L. Li, “Single fed low profile broadband circularly polarized stacked patch antenna,” *IEEE Transactions on Antennas and Propagation*, Vol. 62, No. 10, 5406–5410, Oct. 2014.
4. Yang, W., W.-J. Sun, W. Qin, J.-X. Chen, and J.-Y. Zhou, “Broadband circularly polarized stacked patch antenna with integrated dual feed network,” *IET Microwave and Antennas Propagation*, Vol. 11, No. 12, 1791–1795, 2017.
5. Nasimuddin, X. Qing, and Z. N. Chen, “A wideband circularly polarized stacked slotted microstrip patch antenna,” *IEEE Antennas and Propagation Magazine*, Vol. 55, No. 6, Dec. 2013.
6. Kumar, G. and K. P. Ray, *Broadband Microstrip Antennas*, Artech House, Norwood, MA, 2003.
7. Deshmukh, A. A., A. Parvez, P. Verma, A. Desai, P. Kadam, and K. P. Ray, “Space fed ring microstrip antenna array with stacked rectangular microstrip antenna feed,” *IEEE Annual India Conference (INDICON)*, ISSN: 2325-9418, Feb. 2017.
8. Mathur, P. and G. Kumar, “Non radiating edge coupled rectangular microstrip antenna array,” *IEEE Asia-Pacific Microwave Conference*, ISSN: 2165-4743, 2017.

9. Kumar, H. and G. Kumar, "Compact planar Yagi-Uda antenna with improved characteristics," *11th Euro-pean Conference*, 2017.
10. Hao, Y., G. Wang, Y. Tian, Y. Wang, L. Yu, and X. Ye, "Wide beamwidth circularly polarized microstrip Yagi array antenna," *IEEE International Confrencece on Communication Problem-Solving (ICCP)*, Apr. 2016.
11. Li, Y., S. Sun, and F. Yang, "Miniaturized Yagi-Uda-oriented double-ring antenna with circular polarization and directional pattern," *IEEE Antennas and Wireless Propag. Lett.*, Vol. 12, 945–948, 2013.
12. Zhou, W., J. Liu, and Y. Long, "A broadband and high-gain planar complementary Yagi array antenna with circular polarization," *IEEE Transactions on Antennas and Propagation*, Vol. 65, No. 3, 1446–1451, Jan. 2017.
13. Vaidya, A. R., R. K. Gupta, S. K. Mishra, and J. Mukherjee, "Right-hand/left-hand circularly polarized high-gain antennas using partially reflective surfaces," *IEEE Antennas and Wireless Propag. Lett.*, Vol. 13, 431–434, 2014.
14. Ji, L.-Y., P.-Y. Qin, and Y. Jay Guo, "Wideband Fabry-Perot cavity antenna with a shaped ground plane," *IEEE Access*, Vol. 6, 2291–2297, 2018.
15. Wang, N., J. Li, G. Wei, L. Talbi, Q. Zeng, and J. Xu, "Wideband Fabry-Perot resonator antenna with two layers of dielectric superstrates," *IEEE Antennas Wireless and Propag. Lett.*, Vol. 14, 229–232, 2015.
16. Samanta, G. and S. R. Bhadra Choudhuri, "Design of a compact CP antenna with enhanced bandwidth using a novel hexagonal ring based reactive impedance substrate," *Progress In Electromagnetics Research M*, Vol. 69, 115–125, 2018.